SCIENTIFIC REPORTS

OPEN

SUBJECT AREAS:
HIV INFECTIONS
COMPUTATIONAL MODELS
DEFORMATION DYNAMICS
PROTEIN FUNCTION PREDICTIONS

Received
13 November 2013

Accepted
29 January 2014

Published
13 February 2014

Correspondence and requests for materials should be addressed to B.D.W. (bwalker@partners.org) or R.H.Z. (ruhongz@us.ibm.com)

* These authors contributed equally to this work.

The complex and specific pMHC interactions with diverse HIV-1 TCR clonotypes reveal a structural basis for alterations in CTL function

Zhen Xia[1]*, Huabiao Chen[2]*, Seung-gu Kang[1], Tien Huynh[1], Justin W. Fang[2], Pedro A. Lamothe[2], Bruce D. Walker[2,3] & Ruhong Zhou[1,4]

[1]Computational Biology Center, IBM Thomas J. Watson Research Center, Yorktown Heights, New York, USA, [2]Ragon Institute of Massachusetts General Hospital, Massachusetts Institute of Technology, and Harvard University, Cambridge, Massachusetts, USA, [3]Howard Hughes Medical Institute, Chevy Chase, Maryland, USA, [4]Department of Chemistry, Columbia University, New York, New York, USA.

Immune control of viral infections is modulated by diverse T cell receptor (TCR) clonotypes engaging peptide-MHC class I complexes on infected cells, but the relationship between TCR structure and antiviral function is unclear. Here we apply *in silico* molecular modeling with *in vivo* mutagenesis studies to investigate TCR-pMHC interactions from multiple CTL clonotypes specific for a well-defined HIV-1 epitope. Our molecular dynamics simulations of viral peptide-HLA-TCR complexes, based on two independent co-crystal structure templates, reveal that effective and ineffective clonotypes bind to the terminal portions of the peptide-MHC through similar salt bridges, but their hydrophobic side-chain packings can be very different, which accounts for the major part of the differences among these clonotypes. Non-specific hydrogen bonding to viral peptide also accommodates greater epitope variants. Furthermore, free energy perturbation calculations for point mutations on the viral peptide KK10 show excellent agreement with *in vivo* mutagenesis assays, with new predictions confirmed by additional experiments. These findings indicate a direct structural basis for heterogeneous CTL antiviral function.

Chronic viral infections in mice and humans are modulated by cytotoxic T lymphocyte (CTL)-mediated immune pressure, but the level of immune control is quite variable. This is particularly apparent with HIV-1, a chronic human viral infection that undergoes rapid sequence variation under CTL-mediated immune pressure (see details in a recent review[1]). Immune escape is impeded by the elicitation of a diverse T cell response consisting of multiple specificities[2,3], but these can vary significantly in antiviral efficacy[4–6]. Some induced responses effectively target both wild-type (WT) virus and naturally arising mutants, impeding the development of immune escape[7–9]. Others are readily detectable by tetramer staining, but exhibit little antiviral function *in vitro*, and appear to exert little immune selection pressure *in vivo*[7].

These differences among CTL clonotypes in potency and cross-reactivity of recognition of HIV-1 and its variants[7] are in line with the T cell receptor (TCR)-based modulation of effector cell subsets[10] and suggest that the fine specificity of TCRs may modulate their antiviral function[7,8,11–13]. Although a co-crystalized X-ray structure has recently been reported for a single clonotype interacting with the human leukocyte antigen (HLA) B*2705-restricted epitope KK10 (KRWIILGLNK, Gag aa 263–272)[11], the underlying molecular mechanism for clonotypic differences in antiviral efficacy against this and other epitopes has not been fully understood due to the limited availability of co-crystalized structures of the TCR-peptide-MHC complexes.

In this study, we used a combined approach employing both experimental and theoretical techniques to address the relationship between HIV-1 peptide (KK10)-HLA-TCR complex structure and function. We took advantage of unique reagents generated from persons with untreated HIV-1 infection: intrapatient CTL clones with distinct TCR clonotypes, all induced *in vivo* against the same HLA B*2705-restricted epitope in Gag, but differing in measures of antiviral function. Using molecular dynamics (MD) simulations coupled with functional assays, we show that specific binding patterns among KK10-HLA (B*2705)-TCR interactions are associated with enhanced antiviral efficacy and cross-reactivity of the clonotypes.

Results

Antiviral function of KK10-specific clonotypes. Previously established HLA-B*2705 KK10-specific CTL clonotypes B3, B5 and B6 derived from an HIV-1 controller (FW56) were used in these studies. All clonotypes had considerable sequence diversity in TCR complementarity determining regions (CDRs), and differed in Vβ and Vα gene usage[7] (Table S1). For example, the sequence identities are only ~30% between clones B3, B5, and between clones B5, B6 (Table S2). These clones represented both dominant and subdominant clonotypes present *in vivo*, but differed markedly in their ability to inhibit virus replication *in vitro*[7]. Repeated testing using cryopreserved samples revealed that these clonotypes maintained stable differences in their ability to recognize CD4 T cells infected with HIV-1, as shown in the specific lysis assays (Fig. 1A). It is clear that clonotype B5 broadly recognized the WT and its variant viruses, whereas B3 robustly recognized WT virus but showed little cross-reactivity against variants. In contrast, B6 exhibited weak and narrow recognition. The molecular or structural basis for this diversity among different clonotypes is still largely unknown, which is the main focus of the following large scale molecular modeling.

Structural modeling of TCR-pMHC interaction. Having defined clonotypic difference of antiviral efficacy, we next examined structural properties of effective and ineffective clonotypes in an attempt to relate function to structure. Computational methods have been widely used in structural modeling of biomolecular complexes. In particular, template-based models (homology models) have demonstrated high accuracy in protein structure predictions, as shown in recent CASP competitions[14,15]. Meanwhile, large-scale free energy perturbation (FEP) is regarded as the most rigorous and reliable method in predicting binding affinities, which has also achieved high accuracy in characterizing key residues and their mutational effects for many protein-protein and protein–ligand bindings, as compared with experiments[16–18]. We thus went on to investigate the structural features, dynamic properties, and mutational effects of the ternary binding complexes of KK10-HLA (B*2705)-TCR with computational techniques. Here we used two independent co-crystal structures as templates (more below) to construct homology models of the ternary binding complexes for each FW56 TCR clonotype (see Materials and Methods section for more details), which does not have a crystal structure yet. Considering the high sequence diversities among these TCR clonotypes, it is also difficult, if not impossible, to experimentally determine all KK10-HLA-TCR complex structures here. After the modeling construction, we then performed an aggregate of microsecond MD simulations of these complexes in explicit solvent using IBM Blue Gene supercomputers, which allows us to study their dynamics with atomic resolution. The sensitivity to viral peptide mutants of various clonotypes was also quantitatively measured by calculating their binding affinity changes with FEP (more below).

One representative model of the complex structure for the clonotype B5 is shown in Fig. 2. The viral peptide fits well into the binding groove formed at the interface of the HLA and the TCR. Extensive MD simulations also indicate that these model structures

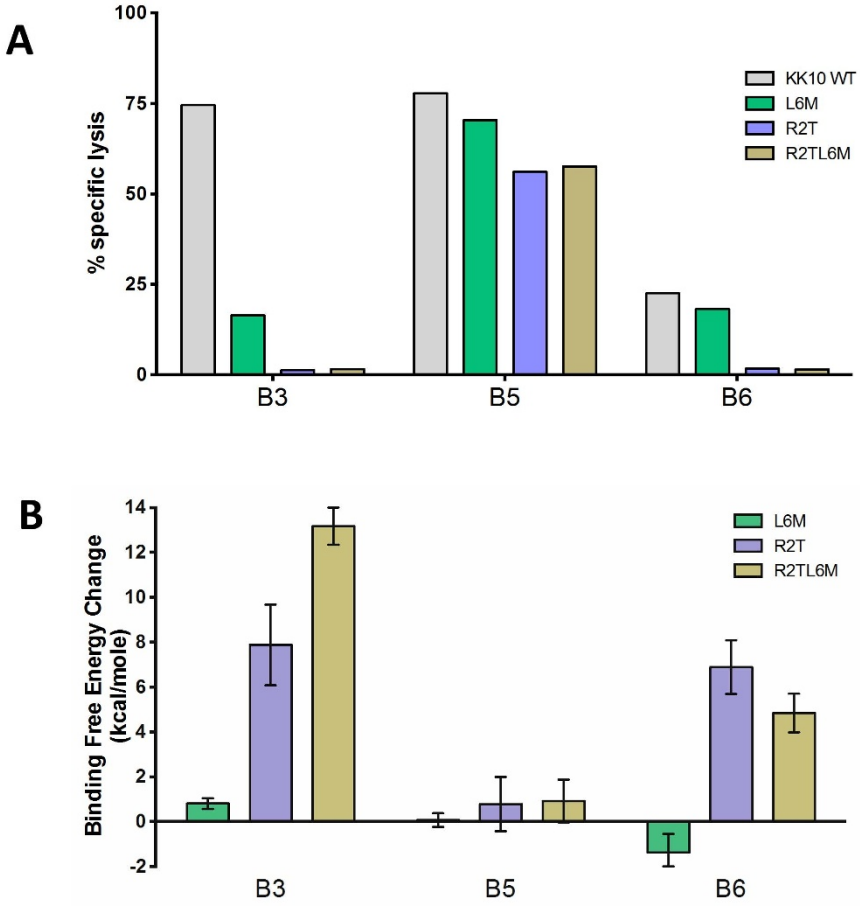

Figure 1 | Differential antiviral efficacy of B*27-KK10 specific clonotypes. (A). The ability of KK10-specific clonotypes to recognize NL4-3 wild-type and variant viruses was tested in the standard 4-h chromium release assay with virally infected HLA-B*2705-encoding green fluorescent protein (GFP) reporter GXR cells at an effector/target cell ratio of 1 : 1. Viable infected (GFP-positive) GXR cells were sorted by a FACS Aria cell-sorting instrument after infection for 5 days and used as target cells. (B). The FEP simulation results for the predicted TCR-KK10 binding free energy change due to L6M and R2T single mutations, and R2TL6M double mutation in viral peptide KK10.

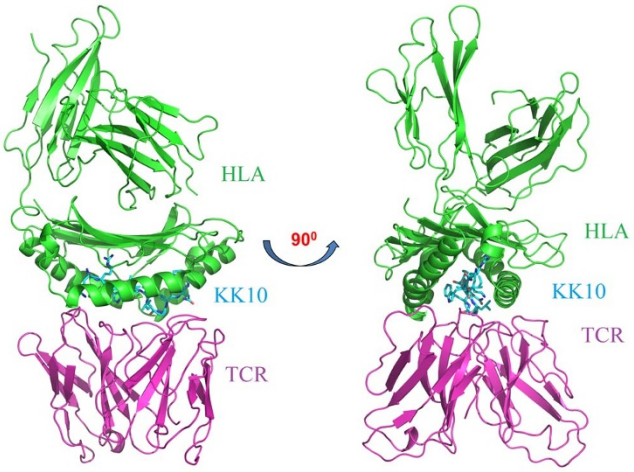

Figure 2 | Structural view of HLA B*2705-KK10-TCR 3-way binding complex. The HLA-B*2705 is shown in green; the KK10 viral peptide is colored in cyan; and the TCR is colored in magenta. All the structural figures are generated with PyMol software.

of clonotypes B3, B5 and B6 are stable, as shown by RMSDs (Fig. S1), indicating a reasonable construction of homology models.

Conserved binding features for functionally different clonotypes. The simulated structures revealed a similar binding mode (binding pocket) on TCRs for KK10-HLA over all clonotypes examined, with more than 20 residues from both the TCR and the HLA-KK10 binary complex involved at the binding site (Fig. 3). We first examined interactions involving the N and C termini of the viral peptide KK10. Although the sequence of the TCR α chain in the clonotype B5 is different from that in clonotypes B3 and B6, we found three common salt-bridges in all clonotypes at the N-terminus of KK10: Lys1 of KK10 with Glu63 of HLA, Arg2 of KK10 with Glu45 of HLA, and Lys1 of KK10 with Asp27/29 at CDR1α loop of the TCR. In particular, for the effective clonotypes B3 and B5, KK10 is further stabilized by extra hydrogen bonds between Glu45/Glu63 of HLA and the amide group at the N-terminus of KK10 (Fig. 3A). The Glu63 at the B pocket of HLA was also recently recognized by genome-wide association analysis (GWAS) as one of the key residues in the single-nucleotide polymorphism of HIV-1 controllers and progressors[19,20]. Similarly, favorable electrostatic interactions contribute to the C-terminal stabilization of the viral peptide. A salt-bridge between Lys10 of KK10 and Asp77 of HLA is found across all clonotypes, while Asn9 of KK10 provides additional stability *via* hydrogen bonds with polar/charged residues from the CDRβ of the TCR (Fig. 3B). Thus, conserved and well-organized salt-bridges and hydrogen bonds play an important role in securing KK10 tightly into the binding pocket between the HLAs and the TCRs. These common N- and C-terminal features contribute to the overall binding affinity between KK10-HLA and TCRs in all clonotypes examined.

Specific hydrophobic packing patterns determine the antiviral efficacy and sensitivity to viral peptide mutants of the clonotypes. Contrary to the highly conserved interactions with the terminal residues of KK10, the central residues are shown to have a more diverse and sophisticated interaction with the CDR loops of TCRs, thus endowing clonotypes B3, B5, and B6 with distinct interactive features. The clonotype B3, effective against WT KK10, has a well-defined hydrophobic packing between the viral peptide and the CDR3β of the TCR (Fig. 3C), where Leu6 and Leu8 of KK10 form favorable contacts with Pro96 and Leu98 of the CDR3β, respectively. The hydrophobic interaction is further enhanced by the additional contacts with hydrophobic residues Ile66, Ala69, and Val152 of the HLA. The formation of a stable hydrophobic core, accompanied by a lower desolvation penalty, makes the B3 TCR and pMHC association more specific. Furthermore, such hydrophobic core (or cavity) formed by nanoscale dewetting (drying) was suggested to provide a substantial driving force for protein complex collapse and overall stability in our previous studies[21–23]. This strong and specific hydrophobic interactions in B3 clonotype (KK10-Leu6 with B3 TCR's Pro96, KK10-Leu8 with B3 TCR's Leu98; see Fig. 3) not only indicates high antiviral efficacy of B3 to the WT virus, but also implies a potentially relatively weak cross-reactivity against variants (i.e. more sensitive to mutants; see more below), as was seen experimentally.

In order to further assess the sensitivity to viral peptide mutants of clonotype B3, which was effective against WT virus but less so against mutants, we calculated binding affinity changes due to mutations frequently occurring *in vivo* (i.e., L6M, R2T and R2TL6M) in KK10 (Fig. 1B). Overall, our *in silico* mutagenesis studies show excellent agreement with those *in vivo* data. Our rigorous FEP calculations show a dramatic weakening in the binding affinities for both R2T ($\Delta\Delta G$ = 7.88 ± 1.80 kcal/mol) and R2TL6M ($\Delta\Delta G$ = 13.17 ± 0.83 kcal/mol) mutants, albeit a somewhat milder reduction in the single L6M mutation ($\Delta\Delta G$ = 0.81 ± 0.24 kcal/mol, which is equivalent to a ~4-fold increase of the dissociation constant *Kd*) (see Table S3), consistent with the specific lysis assay data (Fig. 1A). For more details, the structural comparison reveals that the L6M variant introduces a relatively less hydrophobic side chain to position 6 of KK10, which slightly weakens the well-packed hydrophobic core formed in the WT peptide (Fig. 4A), while the R2T mutant directly destroys the highly conserved salt-bridge between Arg2 in KK10 and Glu45 in HLA. Moreover, the R2T mutation also indirectly loosens another important salt-bridge between Lys1 in KK10 and Asp29 at the CDR1α of the TCR through conformational distortion (Fig. 4B). The even larger decrease in binding affinity for the R2TL6M double mutant is found to be related to larger conformational distortions and serious damage in conserved "signature salt-bridges" (Fig. 4C and 4D).

The binding between the clonotype B5, which is potent against WT virus and variants (see Fig. 1A), and the central residues of KK10 is more complicated due to combined effects of both specific side-chain and non-specific backbone interactions (Fig. 3C). In WT KK10, Leu6 makes hydrophobic contacts with Tyr31 in the CDR1β and Val50 in the CDR2β of the TCR. Meanwhile, Gln98 in the CDR3β forms three hydrogen bonds with nitrogen in the indole ring of Trp3, and backbone carbonyl groups of Leu6 and Gly7 of KK10, respectively. These hydrogen bonds are considered as energetically favored, which could enhance the binding affinity between TCR and KK10. We note that two of the hydrogen bonds are formed with the backbone of KK10 (Gly7 with B5 TCR's Gln98), indicating a lesser sensitivity to the side-chain variations of KK10 (they only interact with the backbone amide and carbonyl groups) (Fig. 3C), which is different from the very specific hydrophobic interaction patterns in B3 clonotype.

These structural observations explain why the clonotype B3 has higher sensitivity to viral peptide mutants against HIV-1 *in vivo* mutants than the clonotype B5. Our FEP study of the clonotype B5 further confirms this (Fig. 1B), in that there is no apparent binding affinity change in the mutant peptide L6M ($\Delta\Delta G$ = 0.07 ± 0.30 kcal/mol), and slightly unfavorable changes in R2T ($\Delta\Delta G$ = 0.78 ± 1.21 kcal/mol) and R2TL6M ($\Delta\Delta G$ = 0.92 ± 0.95 kcal/mol) mutants (Table S3), again in excellent agreement with the *in vitro* experiment. The structural comparisons between these mutants also reveal that the key interactions observed in the WT KK10 peptide are well preserved with no observable binding mode change (Fig. S2), providing a structural basis for the superior efficacy of the clonotype B5 over the broad viral mutations.

The interaction between the least effective clonotype, B6, and WT KK10 peptide is less complex. Only two hydrogen bonds are available

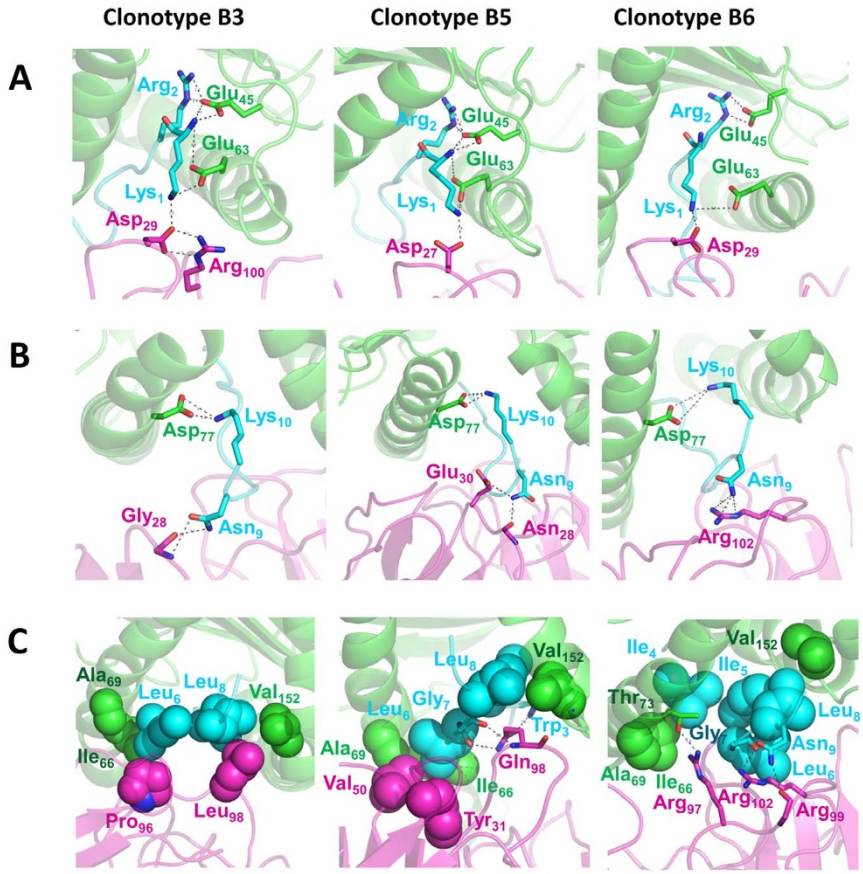

Figure 3 | Structural comparison of different clonotypes bound to the KK10 peptide. The binding site and interactions at the N-terminal region (A), the C-terminal region (B), and the middle region (C) of KK10 peptide are rendered with spheres (non-polar interactions) or sticks (polar interactions) (green, HLA; cyan, HIV-1 KK10 peptide; magenta, TCR). The overall complexes are represented as cartoons. The representative snapshots were taken from totally 600-ns molecular dynamic simulations.

between the CDR3β of the TCR (Arg99 and Arg102) and KK10 peptide (the backbone of Gly7, and the side chain of Asn9, see Fig. 3C). The relatively weak antiviral efficacy, shown in the functional lysis assay (Fig. 1A), is consistent with a lack of favorable hydrophobic interaction, as compared to the clonotypes B3 and B5 (Fig. 3C; also see Fig. S3 and Note 1 in supplementary data).

Alanine substitutions further confirm the structural basis for antiviral efficacy. These *in silico* data suggest specific molecular interactions that modulate antiviral efficacy of specific clonotypes. We next extended the FEP calculations with alanine substitutions (R2A, L6A and R2AL6A) in KK10 peptide, to further investigate the structural basis and intrinsic roles of these important residues in the binding specificity and functional attributes of these clonotypes. Overall, the alanine mutants display a similar trend in binding affinity changes as those naturally occurring mutants (Table S4). For the clonotype B3, the binding affinity is slightly reduced with the L6A mutant ($\Delta\Delta G$ = 0.50 ± 0.51 kcal/mol) as compared to the L6M mutant (Fig. 5A). Although alanine is a smaller and less hydrophobic residue than the original leucine, it is observed that other hydrophobic residues Ile66 and Ala69 in the HLA can adjust themselves to closely pack with Ile4 of KK10 (Fig. S4A). Similar to the R2T variant, a dramatic decrease in the binding affinity ($\Delta\Delta G$ = 8.13 ± 3.55 kcal/mol) is observed in the R2A mutation, again due to the loss of conserved signature salt-bridges at N-terminus (Fig. S4B). For the clonotype B5, all alanine mutants result in relatively small binding affinity losses, but slightly larger than those *in vivo* mutants L6M, R2T, and R2TL6M (Fig. 5A and Fig. S5), meaning that the low sensitivity to viral peptide mutants is still largely maintained in the alanine mutants in the clonotype B5, as found experimentally. Similarly, the binding affinity changes of alanine mutants in the clonotype B6 are very close to those *in vivo* mutants (Fig. S6, also see Note 2 in supplementary data). These FEP predictions are then confirmed by our experimental data from the specific lysis assay (Fig. 5B), indicating our combined approach can quantitatively measure even small differences in binding affinities, thus revealing a direct relationship between peptide-HLA-TCR structure and function.

A second co-crystal structure template further confirms our homology models. It should be noted that a new co-crystal structure with the same HLA-KK10 but a different TCR clonotype was recently reported[11]. We repeated the structural modeling process for clonotypes B3, B5 and B6 using this new co-crystal structure as a second template, and found the newly built homology models shared very similar structures, with comparable binding modes for KK10 as those from the previous template[24,25] (Fig. S7). For example, we found similar salt-bridges and polar interactions between TCR and KK10 peptide in different clonotypes, and similar hydrophobic interactions in B3 and B5 clonotypes. We also repeated the FEP calculations for two representative *in vivo* mutants, L6M and R2T in KK10, which again displayed very similar binding affinity changes with the previous case for all the three clonotypes (see data in Table S5). These findings further support our conclusion that specific structural characteristics of epitope-specific clonotypic TCRs modulate TCR engagement and CTL antiviral efficacy.

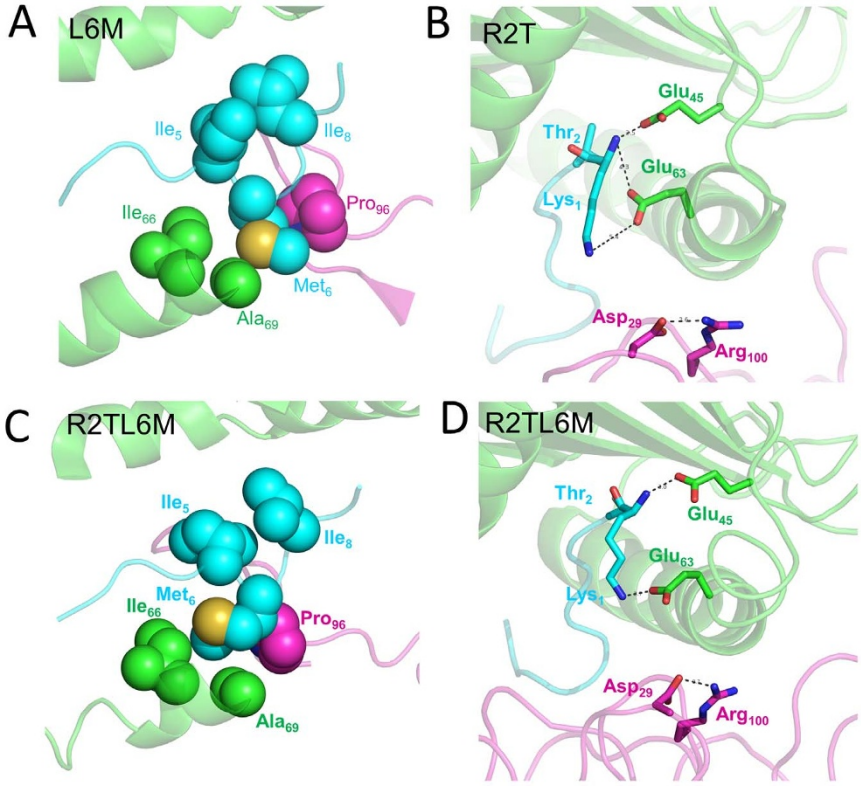

Figure 4 | Structural comparison of HLA B*2705-KK10-TCR complexes due to *in vivo* occurring mutants. The following mutations of KK10 peptide for FW56 clone B3 is shown (green, HLA; cyan, the HIV KK10 peptide; magenta, TCR): (A) L6M mutant. (B) R2T mutant. (C) and (D) R2TL6M double mutant. The overall complex is represented as cartoon and the residues at the binding site are rendered with spheres (non-polar interactions) or sticks (polar interactions).

Discussion

Multiple mechanisms (e.g. the induced-fit model) have been proposed for the TCR and pMHC recognition and binding[25–27]. The TCR-peptide-MHC ternary complex cannot be easily extrapolated from the free peptide-MHC structure, since TCR-peptide recognition is mainly determined by the highly flexible and variable CDR loops. Using a panel of TCR clonotypes specific for the same protective pMHC but differing in antiviral function, we show that conserved polar interactions, including salt-bridges and hydrogen bonds, are presented in both effective and ineffective clonotypes, despite TCR usage of different Vα and Vβ genes. Meanwhile, significantly different packing modes are observed among the clonotypes, especially with the mostly hydrophobic central residues of the viral peptide, which suggests a key role in antiviral efficacy as well as in cross-reactivity.

These studies also allowed us to examine structure and function relationships in the relative ability of different TCR clonotypes to recognize naturally occurring variants within the targeted epitope. CTL-mediated control in rapidly mutating viral infections results from specific TCR-pMHC interactions that trigger antiviral efficacy as well as non-specific interactions that provide a degree of tolerance to the sequence variation of the viral peptide[26,28,29]. Our results using functionally distinct clonotypes from an HIV-1 controller show the impact of the interplay of both specific hydrophobic interactions and non-specific hydrogen bonds in the TCR-viral peptide interaction. In the case examined here, the strong antiviral efficacy of the clonotype B5 is mainly derived from the favorable hydrophobic interactions between the central viral peptide residues and the corresponding hydrophobic residues in the CDR loops. Additionally, the low sensitivity to viral peptide mutants of the clonotype B5 is largely maintained by the strong non-specific hydrogen bonds (also known as dehydrons, which are buried or partially buried hydrogen bonds[30]) between the viral peptide backbone and Gln98 at the CDR3β of the TCR. These dehydrons are energetically very favored, which enhance the binding affinity between KK10 and TCR, resulting in a less sensitivity to mutations. Compared to the clonotype B5, B3's TCR predominantly uses highly specific hydrophobic interactions for contacts with the central residues Leu6 and Leu8 of KK10. This may explain why the high antiviral efficacy is achieved in the clonotype B3, but with a rather high sensitivity to viral peptide variants. There are larger conformational distortions in the clonotype B3 upon mutations. For example, in the R2T mutant, serious damages to the conserved signature salt-bridge (KK10 Lys1 – TCR Asp29) were seen (Figure S8).

These structural analyses were further validated by calculating the binding affinity changes due to point mutations in the viral peptide with the rigorous FEP method. Intrapatient analyses in subject FW56 for clonotypes B3, B5 and B6 showed a clear hierarchy between binding affinity and antiviral efficacy and cross-reactivity. Specific structural alterations accounting for much larger binding affinity losses were found for the KK10 *in vivo* mutants for clonotype B3, indicating a high sensitivity to viral peptide mutants, such as R2T, L6M and R2TL6M, which was confirmed by *in silico* FEP calculations. Additional FEP predictions for all the corresponding alanine substitutions were then further validated by *in silico* mutagenesis studies. The excellent agreements between *in silico* and *in vivo* mutagenesis studies indicate our current structural models and analyses might be reasonable. In particular, our FEP calculations successfully predicted a larger binding affinity change for L6A and R2A mutants than those naturally occurring L6M and R2T ones in the KK10 peptide with the clonotype B5, which were confirmed by our experimental assays. These findings are consistent with recent studies showing that TCR composition and associated signaling potential may modulate effector cell patterning[10].

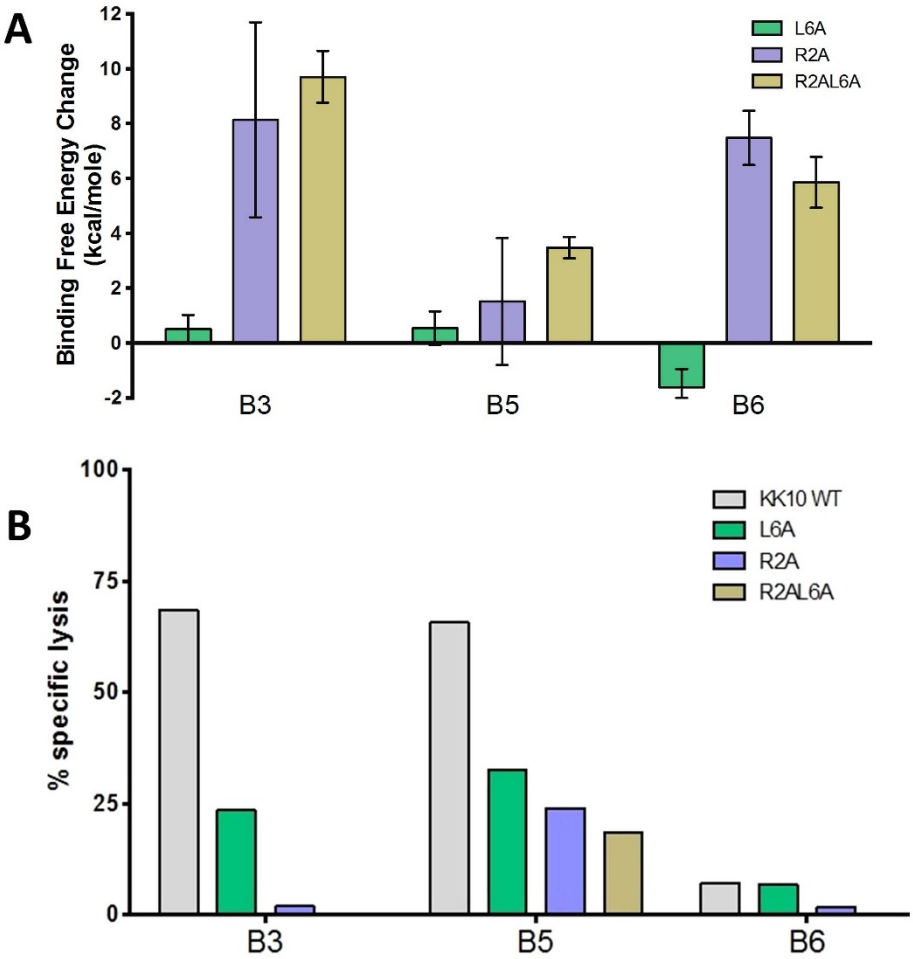

Figure 5 | Impact of alanine substitutions on FEP and antiviral efficacy. (A). The FEP simulation results for the predicted TCR-KK10 binding free energy change due to L6A and R2A single mutations, and R2AL6A double mutation in viral peptide KK10. (B). The ability of KK10-specific clonotypes to recognize KK10 WT peptide and alanine mutants was tested in the standard 4-h chromium release assay with peptide-loaded HLA-B*2705-expressing GXR cells at an effector/target cell ratio of 1 : 1.

We conclude that by applying rigorous binding affinity prediction tools with *in vivo* mutagenesis studies, we not only capture structural and energetic details of particular substitutions, but also reveal the underlying molecular mechanism for differences among TCR clonotypes in their potency and cross-reactivity. This study provides structural and mechanistic insights into T cell-mediated antiviral immunity in a chronic human viral infection.

Methods

Chromium release assay. HLA-B*2705-expressing green fluorescent protein (GFP) reporter CEM-derived GXR cells (which contain a plasmid encoding GFP driven by the long terminal repeat of HIV-1) were constructed as described[31] and infected with the NL4-3 virus or viral variants expressing one or more mutations in the gene encoding Gag p24 KK10 peptide (KRWIILGLNK, Gag aa 263–272) by site-directed mutagenesis[32] at the specified multiplicity of infection (MOI). On day 5 after infection, viable virally infected cells were sorted on a FACS Aria cell-sorting instrument (BD Biosciences) and labeled with chromium for 1 hr at 37°C. CTL clones were then added at the indicated effector-target ratios, and a standard 4-h chromium release assay was performed as previously described[33]. Percent specific lysis was calculated as [(mean experimental cpm − mean spontaneous cpm)/(mean maximum cpm − mean spontaneous cpm)] × 100. Spontaneous and maximum releases were determined by incubating the labeled target cells with medium alone or 2% Triton X-100, respectively.

Structural modeling of HLA B*2705-KK10-TCR complexes. Two independent templates were used in our homology structure modeling for the viral peptide-HLA-TCR complexes. For the first template, the binary structure of HLA B*2705 and KK10 peptide (KRWIILGLNK) complex was taken directly from the co-crystallized x-ray structure (PDB entry 2BSS)[34]. The structures of three different TCR clonotypes, TCRBV4-3 (B3), TRBV6-5 (B5), and TRBV20-1 (B6) of a controller FW56, were built from their closest homologs, with MODELLER software package[35,36], based on TCR sequence details from the respective clonotypes B3, B5, and B6 (Table S1). After that, the entire complex was aligned to an available ternary complex (PDB entry 3H9S)[25]. The binding interface between complementarity determining regions (CDRs) of TCR and the KK10 peptide was optimized globally at atomic level by a Potential Smoothing and Search method in TINKER package[37]. The second template followed a similar procedure, but with a newly released co-crystal structure (PDB entry: 4G8G) as the input (see main text).

Molecular dynamics simulations. Each HLA B*2705-KK10-TCR complex was solvated in a 77.5 Å × 128.0 Å × 76.5 Å water box, where the system was firstly neutralized with counter ions, and then further ionized in a 150 mM NaCl in order to mimic *in vivo* physiological environment. The solvated system was minimized by 20,000 steps, then followed by a ~1 ns equilibration (with a 0.5-fs timestep) in 1 atm and 310 K. In each system, five snapshots at the second half of the equilibration were randomly picked as starting structures for up to 50 ns long molecular dynamics simulations and independent 60 + ns free energy perturbation (FEP) calculations for each system, with an aggregate of 1.7 microseconds MD simulation time for all clonotypes and their variants. The unbound (free) state of the FEP calculation was modeled with the binary complex of only HLA-KK10, which was prepared with a similar protocol employed for the bound system of HLA B*2705-KK10-TCR complex. The particle-mesh Ewald (PME) method was used for the long-range electrostatic interactions[38], while the van der Waals interactions were handled with usual smooth cutoff with a cutoff distance of 12 Å. All molecular dynamics simulations have been performed with a specially optimized NAMD2 molecular modeling package for Blue Gene[39,40], with a 1.5-fs timestep in NPT ensemble at 1 atom and 310 K. Molecular dynamics simulations have been widely used in modeling biological systems to complement experiments, which can provide atomic details that are often inaccessible in experiments due to resolution limits even with the current most sophisticated experimental techniques[22,41–50]. The CHARMM22 force field[51] and TIP3P water model[52] are used for proteins and solvents, respectively.

Free energy perturbation protocol. The binding affinity changes, due to antigenic variations, between the TCR and HLA-KK10 complex were estimated by the free energy perturbation (FEP) method[16,17,53–60]. We calculate the free energy changes for the same mutation(s) in both the bound state (HLA-KK10-TCR 3-way binding complex) and the free state (HLA-KK10 binary complex). For each mutation, at least five independent runs starting from different initial configurations (taken from the molecular dynamic simulations) are performed for better sampling. The simulation time for each run is 6.0 ns, thus, at least 60 ns (6.0-ns × 5-runs × 2-states) simulation time was generated for each mutation. Larger window sizes and longer simulation durations have also been tested in our previous studies, and we found that the current protocol gives us a reasonable convergence in the final binding affinities[16,18]. Please see Note 3 in supporting data for more detailed description of the FEP protocol.

1. McMichael, A. J., Borrow, P., Tomaras, G. D., Goonetilleke, N. & Haynes, B. F. The immune response during acute HIV-1 infection: clues for vaccine development. *Nat. Rev. Immunol.* **10**, 11–23 (2010).
2. Addo, M. M. *et al.* Comprehensive epitope analysis of human immunodeficiency virus type 1 (HIV-1)-specific T-cell responses directed against the entire expressed HIV-1 genome demonstrate broadly directed responses, but no correlation to viral load. *J. Virol.* **77**, 2081–92 (2003).
3. Betts, M. R. *et al.* Analysis of total human immunodeficiency virus (HIV)-specific CD4(+) and CD8(+) T-cell responses: relationship to viral load in untreated HIV infection. *J. Virol.* **75**, 11983–91 (2001).
4. Kiepiela, P. *et al.* CD8+ T-cell responses to different HIV proteins have discordant associations with viral load. *Nat. Med.* **13**, 46–53 (2007).
5. Harari, A. *et al.* Skewed association of polyfunctional antigen-specific CD8 T cell populations with HLA-B genotype. *Proc. Natl. Acad. Sci. U. S. A.* **104**, 16233–8 (2007).
6. Chen, H. *et al.* Differential neutralization of human immunodeficiency virus (HIV) replication in autologous CD4 T cells by HIV-specific cytotoxic T lymphocytes. *J. Virol.* **83**, 3138–49 (2009).
7. Chen, H. *et al.* TCR clonotypes modulate the protective effect of HLA class I molecules in HIV-1 infection. *Nat. Immunol.* **13**, 691–700 (2012).
8. Iglesias, M. C. *et al.* Escape from highly effective public CD8+ T-cell clonotypes by HIV. *Blood* **118**, 2138–49 (2011).
9. Allen, T. M. *et al.* De novo generation of escape variant-specific CD8+ T-cell responses following cytotoxic T-lymphocyte escape in chronic human immunodeficiency virus type 1 infection. *J. Virol.* **79**, 12952–60 (2005).
10. Tubo Noah, J. *et al.* Single Naive CD4+ T Cells from a Diverse Repertoire Produce Different Effector Cell Types during Infection. *Cell* **153**, 785–796 (2013).
11. Ladell, K. *et al.* A Molecular Basis for the Control of Preimmune Escape Variants by HIV-Specific CD8(+) T Cells. *Immunity* **38**, 425–36 (2013).
12. Mendoza, D. *et al.* HLA B*5701-positive long-term nonprogressors/elite controllers are not distinguished from progressors by the clonal composition of HIV-specific CD8+ T cells. *J. Virol.* **86**, 4014–8 (2012).
13. Janbazian, L. *et al.* Clonotype and repertoire changes drive the functional improvement of HIV-specific CD8 T cell populations under conditions of limited antigenic stimulation. *J. Immunol.* **188**, 1156–67 (2012).
14. Cozzetto, D. *et al.* Evaluation of template-based models in CASP8 with standard measures. *Proteins* **77**, 18–28 (2009).
15. Mariani, V., Kiefer, F., Schmidt, T., Haas, J. & Schwede, T. Assessment of template based protein structure predictions in CASP9. *Proteins* **79**, 37–58 (2011).
16. Zhou, R., Das, P. & Royyuru, A. K. Single Mutation Induced H3N2 Hemagglutinin Antibody Neutralization: A Free Energy Perturbation Study. *J. Phys. Chem. B* **112**, 15813–15820 (2008).
17. Das, P., Li, J., Royyuru, A. K. & Zhou, R. Free energy simulations reveal a double mutant avian H5N1 virus hemagglutinin with altered receptor binding specificity. *J. Comput. Chem.* **30**, 1654–1663 (2009).
18. Xia, Z., Huynh, T., Kang, S. G. & Zhou, R. Free-energy simulations reveal that both hydrophobic and polar interactions are important for influenza hemagglutinin antibody binding. *Biophys J* **102**, 1453–61 (2012).
19. Pereyra, F. P. *et al.* The Major Genetic Determinants of HIV-1 Control Affect HLA Class I Peptide Presentation. *Science* **330**, 1551–1557 (2010).
20. McLaren, P. J. *et al.* Fine-mapping classical HLA variation associated with durable host control of HIV-1 infection in African Americans. *Hum. Mol. Genet.* (2012).
21. Zhou, R. H., Huang, X. H., Margulis, C. J. & Berne, B. J. Hydrophobic collapse in multidomain protein folding. *Science* **305**, 1605–1609 (2004).
22. Liu, P., Huang, X., Zhou, R. & Berne, B. J. Observation of a dewetting transition in the collapse of the melittin tetramer. *Nature* **437**, 159–62 (2005).
23. Wu, Y., Vadrevu, R., Kathuria, S., Yang, X. & Matthews, C. R. A tightly packed hydrophobic cluster directs the formation of an off-pathway sub-millisecond folding intermediate in the alpha subunit of tryptophan synthase, a TIM barrel protein. *J. Mol. Biol.* **366**, 1624–38 (2007).
24. Kjer-Nielsen, L. *et al.* A structural basis for the selection of dominant alpha beta T cell receptors in antiviral immunity. *Immunity* **18**, 53–64 (2003).
25. Borbulevych, O. Y. *et al.* T Cell Receptor Cross-reactivity Directed by Antigen-Dependent Tuning of Peptide-MHC Molecular Flexibility. *Immunity* **31**, 885–896 (2009).
26. Macdonald, W. A. *et al.* T Cell Allorecognition via Molecular Mimicry. *Immunity* **31**, 897–908 (2009).
27. Yin, Y. Y. & Mariuzza, R. A. The Multiple Mechanisms of T Cell Receptor Cross-reactivity. *Immunity* **31**, 849–851 (2009).
28. Dunn, S. M. *et al.* Directed evolution of human T cell receptor CDR2 residues by phage display dramatically enhances affinity for cognate peptide-MHC without increasing apparent cross-reactivity. *Protein Sci.* **15**, 710–721 (2006).
29. Kjer-Nielsen, L. *et al.* The structure of HLA-B8 complexed to an immunodominant viral determinant: Peptide-induced conformational changes and a mode of MHC class I dimerization. *J. Immunol.* **169**, 5153–5160 (2002).
30. Fernandez, A. & Scheraga, H. A. Insufficiently dehydrated hydrogen bonds as determinants of protein interactions. *Proc. Natl. Acad. Sci. U. S. A.* **100**, 113–118 (2003).
31. Brockman, M. A., Tanzi, G. O., Walker, B. D. & Allen, T. M. Use of a novel GFP reporter cell line to examine replication capacity of CXCR4- and CCR5-tropic HIV-1 by flow cytometry. *J. Virol. Methods* **131**, 134–42 (2006).
32. Schneidewind, A. *et al.* Structural and functional constraints limit options for cytotoxic T-lymphocyte escape in the immunodominant HLA-B27-restricted epitope in human immunodeficiency virus type 1 capsid. *J. Virol.* **82**, 5594–605 (2008).
33. Yang, O. O. *et al.* Impacts of avidity and specificity on the antiviral efficiency of HIV-1-specific CTL. *J. Immunol.* **171**, 3718–24 (2003).
34. Stewart-Jones, G. B. *et al.* Crystal structures and KIR3DL1 recognition of three immunodominant viral peptides complexed to HLA-B*2705. *Eur. J. Immunol.* **35**, 341–51 (2005).
35. Sali, A. & Blundell, T. L. Comparative Protein Modeling by Satisfaction of Spatial Restraints. *J. Mol. Biol.* **234**, 779–815 (1993).
36. Fiser, A., Do, R. K. G. & Sali, A. Modeling of loops in protein structures. *Protein Sci.* **9**, 1753–1773 (2000).
37. Pappu, R. V., Hart, R. K. & Ponder, J. W. Analysis and application of potential energy smoothing and search methods for global optimization. *J. Phys. Chem. B* **102**, 9725–9742 (1998).
38. Darden, T. A., York, D. M. & Pedersen, L. G. Particle mesh Ewald: An NlogN method for Ewald sums in large systems. *J. Chem. Phys.* **98**, 10089–10092 (1993).
39. Kumar, S. *et al.* Scalable Molecular Dynamics with NAMD on Blue Gene/L. *IBM J. Res. Dev.* **52**, 177–188 (2008).
40. Morrone, J. A., Zhou, R. H. & Berne, B. J. Molecular Dynamics with Multiple Time Scales: How to Avoid Pitfalls. *J. Chem. Theo. Comp.* **6**, 1798–1804 (2010).
41. Eleftheriou, M., Germain, R. S., Royyuru, A. K. & Zhou, R. Thermal denaturing of mutant lysozyme with both the OPLSAA and the CHARMM force fields. *J. Am. Chem. Soc.* **128**, 13388–95 (2006).
42. Zhou, R., Berne, B. J. & Germain, R. The free energy landscape for beta hairpin folding in explicit water. *Proc Natl Acad Sci U S A* **98**, 14931–6 (2001).
43. Zhou, R., Eleftheriou, M., Royyuru, A. K. & Berne, B. J. Destruction of long-range interactions by a single mutation in lysozyme. *Proc Natl Acad Sci U S A* **104**, 5824–9 (2007).
44. Gao, Y. Q., Yang, W. & Karplus, M. A structure-based model for the synthesis and hydrolysis of ATP by F_1-ATPase. *Cell* **123**, 195–205 (2005).
45. Hummer, G., Rasaiah, J. C. & Noworyta, J. P. Water conduction through the hydrophobic channel of a carbon nanotube. *Nature* **414**, 188–190 (2001).
46. Kamberaj, H. & van der Vaart, A. An optimized replica exchange molecular dynamics method. *J. Chem. Phys.* **130**, 074906 (2009).
47. Karplus, M., Gao, Y. Q., Ma, J., van der Vaart, A. & Yang, W. Protein structural transitions and their functional role. *Philos. Transact. A Math. Phys. Eng. Sci.* **363**, 331–355; discussion 355–356 (2005).
48. Zheng, L., Chen, M. & Yang, W. Random walk in orthogonal space to achieve efficient free-energy simulation of complex systems. *Proc. Natl. Acad. Sci. U. S. A.* **105**, 20227–20232 (2008).
49. Fitch, B. G. *et al. Blue Matter: Strong scaling of molecular dynamics on Blue Gene/L*, (Springe rBerlin Heidelberg, 2006).
50. Kaminski, G. A., Friesner, R. A. & Zhou, R. A computationally inexpensive modification of the point dipole electrostatic polarization model for molecular simulations. *J Comput Chem* **24**, 267–76 (2003).
51. MacKerell, A. D. *et al.* All-atom empirical potential for molecular modeling and dynamics studies of proteins. *J. Phys. Chem. B* **102**, 3586–3616 (1998).
52. Jorgensen, W. L., Chandrasekhar, J., Madura, J. D., Impey, R. W. & Klein, M. L. Comparison of simple potential functions for simulating liquid water. *J. Chem. Phys.* **79**, 926–935 (1983).
53. Deng, Y. & Roux, B. Calculation of standard binding free energies: aromatic molecules in the T4 lysozyme L99A mutant. *J. Chem. Theo. Comp.* **2**, 1255–1273 (2006).
54. Jorgensen, W. L. Free-energy calculations - a breakthrough for modeling organic-chemistry in solution. *Acc. Chem. Res.* **22**, 184–189 (1989).
55. Kollman, P. Free-energy calculations - applications to chemical and biochemical phenomena. *Chem. Rev.* **93**, 2395–2417 (1993).
56. Simonson, T., Archontis, G. & Karplus, M. Free energy simulations come of age: Protein-ligand recognition. *Acc. Chem. Res.* **35**, 430–437 (2002).
57. Tembe, B. L. & McCammon, J. A. Ligand receptor interactions. *Computers & Chemistry* **8**, 281–283 (1984).
58. Warshel, A. Simulating the Energetics and Dynamics of Enzymatic Reactions. *Specificity in Biological Interactions* **55**, 59–81 (1984).
59. Warshel, A., Sharma, P. K., Kato, M. & Parson, W. W. Modeling Electrostatic Effects in Proteins. *Biochim. Biophys. Acta* **1764**, 1647–1676 (2006).

60. Xia, Z., Das, P., Huynh, T., Royyuru, A. K. & Zhou, R. Modeling mutations of influenza virus with IBM Blue Gene. *IBM J. Res. Dev.* **55** (2011).

Acknowledgments

This work was supported by the IBM Blue Gene Science Program (R.Z.), the Harvard University Center for AIDS Research (5 P30 AI060354-04), grants from the Bill and Melinda Gates Foundation (B.D.W.), the Doris Duke Charitable Foundation (B.D.W.), the NIH (B.D.W. AI030914), the Howard Hughes Medical Institute (B.D.W.), and the Mark and Lisa Schwartz Foundation (B.D.W.). We also thank IBM Watson Blue Gene Supercomputer Center for computational resources.

Author contributions

R.Z. and B.D.W. conceived and designed the research. Z.X., H.C., S.K., T.H., B.D.W. and R.Z. co-wrote the manuscript. Z.X. and T.H. carried out the computational modeling, molecular dynamics simulations, and free energy calculations. H.C., J.W.F. and P.A.L., carried the chromium release assay. Z.X., H.C., T.H., S.G. and R.Z. analyzed the data. All authors discussed the results and commented on the manuscript.

Additional information

Supplementary information accompanies this paper at http://www.nature.com/scientificreports

Competing financial interests: The authors declare no competing financial interests.

How to cite this article: Xia, Z. *et al.* The complex and specific pMHC interactions with diverse HIV-1 TCR clonotypes reveal a structural basis for alterations in CTL function. *Sci. Rep.* **4**, 4087; DOI:10.1038/srep04087 (2014).